Subwavelength-engineered metamaterial devices for integrated photonics

A. Sánchez-Postigo*[a], P. Ginel-Moreno[a], D. Pereira-Martín[a], A. Hadij-ElHouati[a], J. M. Luque-González[a], C. Pérez-Armenta[a], J. G. Wangüemert-Pérez[a], A. Ortega-Moñux[a], R. Halir[a], J. H. Schmid[b], J. Soler Penadés[c,d], M. Nedeljkovic[c], W. N. Ye[e], G. Z. Mashanovich[c], P. Cheben[b], I. Molina-Fernández[a]

[a]Telecommunication Research Institute (TELMA), Universidad de Málaga, Louis Pasteur 35, 29010 Málaga, Spain; [b]National Research Council Canada, 1200 Montreal Road, Bldg. M50, Ottawa K1A 0R6, Canada; [c]Optoelectronics Research Centre, University of Southampton, Southampton, SO17 1BJ, United Kingdom; [d]VLC Photonics, S. L., Spain; [e]Department of Electronics, Carleton University, 1125 Colonel By Drive, Ottawa, Ontario K1S5B6, Canada

(Invited paper)

ABSTRACT

The engineering of subwavelength grating metamaterials has become an essential design strategy in silicon photonics. The lithographic segmentation of integrated waveguides at the subwavelength scale enables the synthesis of on-chip metamaterials and provides control over optical properties such as mode delocalization, wavelength dispersion, and anisotropy. At the near-infrared wavelengths of the 1.55-μm telecom band, a range of subwavelength-based devices with unprecedented performance has been demonstrated, including couplers, filters, and polarization-handling structures. In this invited paper, we review the foundations of anisotropic subwavelength grating metamaterials and discuss our latest advances in five new subwavelength-enhanced devices: a millimeter-long optical antenna that is evanescently coupled to diffractive lateral segments, thereby achieving a record far-field beam width of 0.1º in silicon; a multi-line integrated Bragg filter also using lateral loading segments, which produces 20 non-uniformly spaced spectral notches with a 3-dB linewidth as low as 210 pm; a low-loss curved wavelength demultiplexer; a segmented multi-mode interference coupler based on novel bricked subwavelength gratings, yielding a 1-dB bandwidth exceeding 140 nm; and a suspended waveguide platform with low propagation loss at mid-infrared wavelengths.

Keywords: silicon photonics, integrated optics, subwavelength grating metamaterials, SWG, optical antennas, Bragg filters, wavelength demultiplexers, mid-infrared

1. INTRODUCTION

The choice of materials in silicon photonics — limited to silicon, silicon dioxide, and silicon nitride — can be expanded by using subwavelength grating (SWG) metamaterials. Since their first experimental demonstration in integrated waveguides by Cheben et al.[1], SWG structures have become an integral design tool in silicon photonics, enabling the development of optical devices with enhanced performance[2–4]. A waveguide core that is segmented at the subwavelength scale (with a period Λ and silicon blocks of length a = DC·Λ, where DC denotes the duty cycle) can be modeled as an equivalent homogeneous anisotropic waveguide core with a permittivity tensor

$$\boldsymbol{\varepsilon}_{\mathrm{eq}} = \begin{pmatrix} n_{xx}^2 & 0 & 0 \\ 0 & n_{yy}^2 & 0 \\ 0 & 0 & n_{zz}^2 \end{pmatrix}, \tag{1}$$

where n_{xx}, n_{yy}, and n_{zz} can be calculated using simple Python or MATLAB scripts[5] as detailed in our review paper[4]. By adequately choosing the geometry of the SWG waveguide (Λ and DC), the tensor components can be tailored, thus

*asp@ic.uma.es; phone 34 952132853; www.photonics-rf.uma.es

facilitating refractive-index, dispersion, and anisotropy engineering. Many components have been demonstrated that use SWG metamaterials to achieve unprecedented performance, including ultra-broadband fiber-chip couplers[6], GRIN-lens spot size converters[7], sensors with increased sensitivity[8–11], and devices to manage polarization[12–14], to name a few. In this paper, we present an overview of our latest advances in subwavelength-engineered devices in silicon photonics.

2. MILLIMETER-LONG SURFACE EMITTING ANTENNA

One of the most common configurations of optical phased arrays (OPAs) uses long sidewall modulated waveguide gratings as optical antennas that are densely packed in the transverse direction[15–18]. By varying the phases of the fields that feed the antennas, it is possible to direct the radiated field at an angle ϕ in the transverse direction (azimuthal angle). On the other hand, beam steering in the longitudinal direction (elevation angle) is achieved by tuning the wavelength, λ, as this parameter strongly affects the radiation angle θ in grating waveguides[19]:

$$\theta = \sin^{-1}\left(\frac{n_B}{n_u} - \frac{\lambda}{n_u \Lambda}\right), \tag{2}$$

where n_B is the effective index of the Bloch mode that is supported by antenna grating, n_u is the refractive index of the upper medium (typically air, $n_u = 1$), and Λ is the period of the antenna perturbation.

The main downside of the 1D-OPA topology is that the radiation strength of the grating antennas must be very low to radiate most of the power in a millimeter scale and hence produce a narrow beamwidth in the far field. In silicon platforms, this requirement imposes extremely small corrugation sizes (on the order of 10 nm), which complicates fabrication in deep-ultra-violet lithography facilities[20]. To circumvent this problem, we have proposed a silicon optical antenna formed by a SWG waveguide core (width W, period Λ_{SWG}) with diffractive silicon segments placed aside (width W_s, length L_s, period Λ_g, separation from core g)[21,22]. The SWG metamaterial allows to accurately delocalize the propagating mode that evanescently overlaps with the lateral segments, in order to reduce the grating strength while maintaining a minimum feature size above 80 nm. Our optical antenna, shown in Fig. 1(a), is fabricated in a 220-nm-thick SOI platform with 2-µm-thick buried oxide (BOX) and has a length of a 2 mm, which leads to a record beam divergence of 0.1° (see Fig. 1(b)) for TE polarization. In our experiments, a wavelength sensitivity of -0.13º/nm is measured. These results are comparable to those of state-of-the-art optical antennas in silicon that use ~10 times smaller feature sizes[15–17].

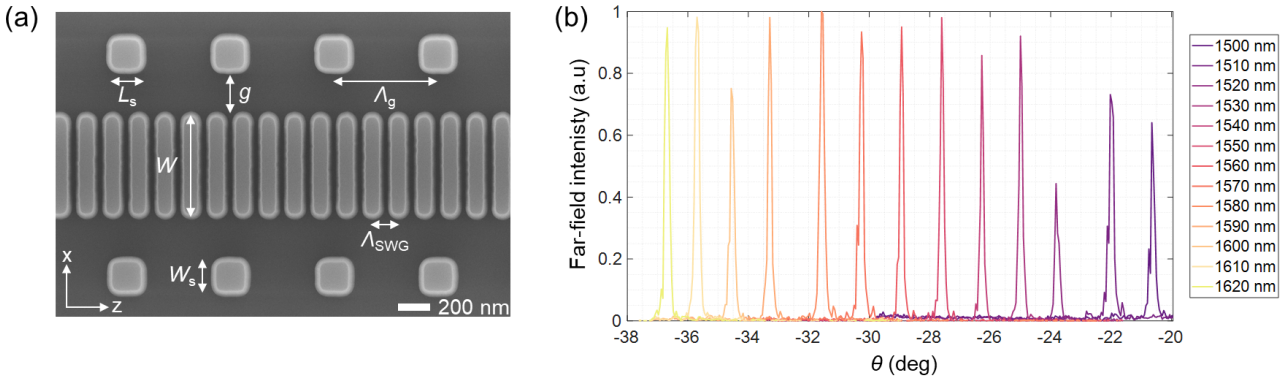

Figure 1. (a) SEM image of a millimeter-long optical antenna with SWG core to delocalize the guided mode and loading segments to enable off-chip radiation. (b) Measured far-field intensity radiated by one optical antenna at longitudinal direction for several wavelengths, yielding a narrow beamwidth of ~0.1º and a scan range of 13º per 100-nm wavelength tuning.

3. MULTI-LINE SPECTRAL FILTER

Typically, integrated Bragg filters have a periodic modulation in a waveguide core that enables light reflection at specific wavelengths. The bandwidth of the filter is primarily determined by the size of the sidewall corrugation. Thus,

most silicon filters with narrowband spectral characteristics require very small feature sizes[23,24], which hinders practical implementation. By appropriately reducing the period length of the lateral segments, the same grating topology that is used to develop optical antennas in Section 2 can be employed to implement silicon Bragg filters with a customized spectral response, as shown in Fig. 2(a)[25]. Here we adjust the duty cycle of the SWG core to delocalize the Bloch guided mode. This increases the separation of the loading segments, such that minimum-feature-size constraints can be satisfied. By using the layer-peeling algorithm[26], we obtain the local reflection coefficients of each Bragg period, ρ_k, that synthesize a target reflection spectrum, which are then mapped onto the lateral separations, s_k, and the Bragg period modulation, Λ_k (see Fig. 2(a)).

Figure 2(b) shows the transmittance spectral response of one of our optical filters, fabricated in a 220-nm-thick SOI platform with 2-μm-thick buried oxide (BOX) layer. The filter is designed to operate with TM polarization, in order to increase the Bloch mode delocalization and the Bragg segment separations, and has a total length of 6.4 mm. The fabricated filter exhibits 20 non-uniformly spaced notches at wavelengths near 1550 nm, matching the target spectrum and yielding a 3-dB linewidth as low as 210 pm and extinction rations up to 11 dB.

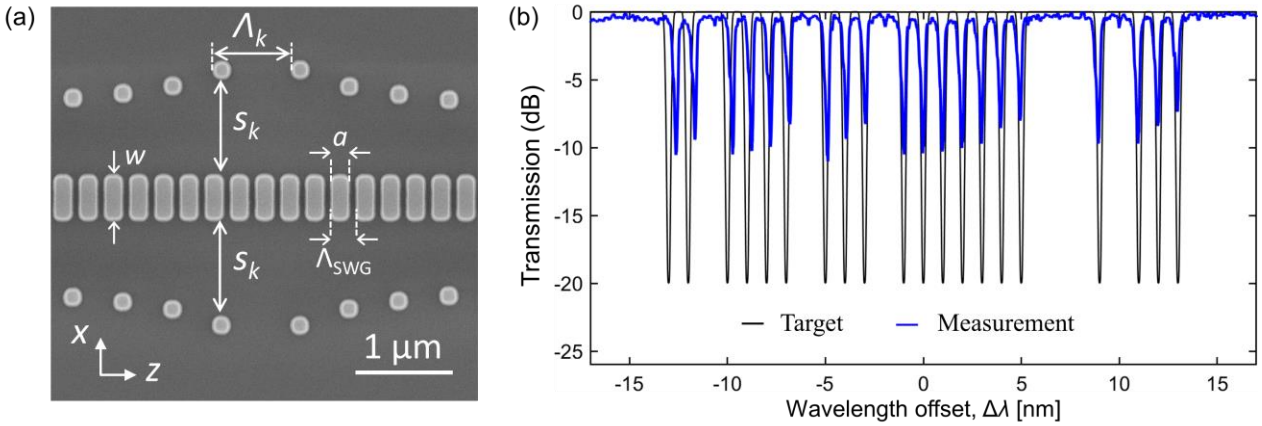

Figure 2. (a) SEM image of an SWG waveguide loaded with lateral Bragg gratings in silicon to produce a customized spectral response using minimum feature sizes of ~100 nm. (b) Target (black) and measured (blue) spectral responses.

4. CURVED WAVELENGTH DEMULTIPLEXER

A CWG demultiplexer comprises a circularly shaped (diameter D) blazed grating waveguide that radiates into a free-propagation region (FPR) slab waveguide[27,28]. At different wavelengths, the radiated field is focused at different points along a focal curve (Rowland circle, diameter $D/2$), at which the output waveguides are positioned, thereby producing wavelength demultiplexing. The first CWG demultiplexer demonstration in SOI used an SWG metamaterial adaptation region to minimize the radiation loss[29]. In that work, the SWG structure successfully reduced the adaptation loss between the waveguide grating and the FPR slab. Nevertheless, the demonstrated device still had high insertion loss (~4 dB), which mainly arose from off-chip radiation into the upper and bottom SiO_2 claddings[30]. To suppress off-chip radiation and hence maximize the amount of power that is coupled into the free-propagation region, we judiciously design the SWG metamaterial lateral cladding such that the grating period, Λ, meets the single-beam condition[31]

$$n_{\mathrm{ub}} + n_{\mathrm{B}} < \frac{\lambda}{\Lambda} < n_{\mathrm{SWG}} + n_{\mathrm{B}}, \tag{3}$$

where n_{ub} is the refractive index of the upper and bottom cladding and n_{SWG} is the synthesized refractive index of the SWG cladding. Using this approach, we have recently demonstrated a low-loss CWG demultiplexer in a 220-nm-thick SOI platform with SiO2 bottom and upper cladding[32]. The nominal period Λ is chosen to satisfy Eq. (3), enabling on-chip radiation at 35º with respect to the vertical at the nominal wavelength of 1550 nm for TE polarization. To maximize the overlap between the radiated field and the mode field of the output waveguide, the radiated field at the grating plane is adequately shaped in both phase and amplitude. For this purpose, the grating is apodized in strength and its pitch is chirped[32].

Fig. 3(a) shows an SEM image of the fabricated device, in which the orange and purple regions represent the focusing beams at the wavelengths of the first and last channels, respectively. Figure 3(b) shows the transmitted power as a function of the wavelength for 11 channels from 1530 nm to 1630 nm with a separation of 10 nm. The best performing output channels (1–6) exhibit insertion losses below 2 dB, with a minimal loss below 1 dB and a crosstalk below -25 dB (channel 2). This device can be effectively used for wavelength division multiplexing (WDM) applications.

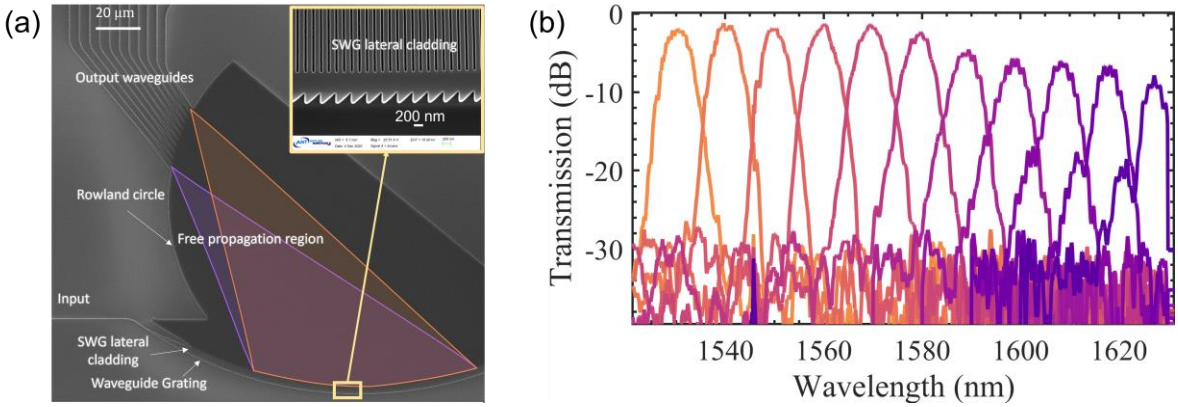

Figure 3. (a) SEM image of a CWG demultiplexer using a conveniently designed SWG metamaterial lateral cladding to frustrate off-chip radiation and minimize insertion loss. (b) Transmitted power as a function of the wavelength. Each color represents an WDM channel.

5. BRICKED SUBWAVELENGTH GRATINGS

Anisotropy engineering of SWG metamaterials allows for the development of optical devices with, e.g., increased bandwidth or polarization-dependent properties[33–35]. In 2019, we proposed tilted subwavelength gratings (see Fig. 4(a)) as a means of affecting the horizontal tensor components, which mainly influence TE (in-plane) polarization, while leaving n_{yy} virtually unchanged[36–38]. In this tilted SWG metamaterial, the period Λ of the grating is maintained in the tilted axis and the period is therefore increased in the propagation direction by a factor of $1/\cos(\theta)$. As a result, the wavelength at which the grating enters the Bragg regime is barely altered compared to conventional, non-tilted subwavelength gratings. Recently, we have proposed bricked subwavelength gratings, illustrated in Fig. 4(b), in which the period is maintained in the propagation direction[39]. These gratings are obtained, first, by periodically segmenting the silicon strips of an SWG waveguide in the transverse direction (period Λ_x) and, then, by alternatively shifting the resulting silicon blocks by a length d_z in the propagation direction. In addition to offering similar anisotropy advantages of tilted SWG waveguides, as shown in Fig. 4(c), this topology allows to move the Bragg wavelength condition to shorter wavelengths or, alternatively, to enlarge the period length while maintaining subwavelength behavior[39].

Segmenting a multimode interference (MMI) coupler at the subwavelength scale can flatten the coupling length (L_π) with respect to the wavelength, which results in a substantially enlarged bandwidth[33]. However, in a standard SOI platform, the period that is required to operate in the deep-SWG regime (i.e., far away enough from the Bragg wavelength) with sufficiently low chromatic dispersion is below 200 nm[4]. This period size produces small feature sizes that may complicate fabrication using large-scale deep-ultra-violet lithography. We have utilized our bricked SWG topology to design an ultra-broadband multimode interference (MMI) coupler in 220-nm-thick SOI that operates in the SWG regime with a period of 300 nm[39]. This period length would lead to a prohibitive feature size for conventional (d_z = 0) SWG waveguides. Figure 4(b) shows an SEM image of the fabricated bricked-SWG MMI coupler, which yields excess loss and power imbalance below 1 dB over a wavelength range of 140 nm, limited by our measurement setup (see Fig. 4(d)).

By engineering the anisotropic behavior of a bricked-SWG waveguide, we have also demonstrated a polarization-insensitive ultra-broadband MMI. By using a (period, duty cycle) pair of (250 nm, 60%) in the propagation direction and (200 nm, 50%) in the transverse direction, with a displacement d_z of 120 nm, the L_π lengths for both TE and TM polarizations were matched and the MMI achieved an excess loss below 1 dB, a power imbalance below 1 dB, and a phase error below ±5º in a bandwidth of ~60 nm.

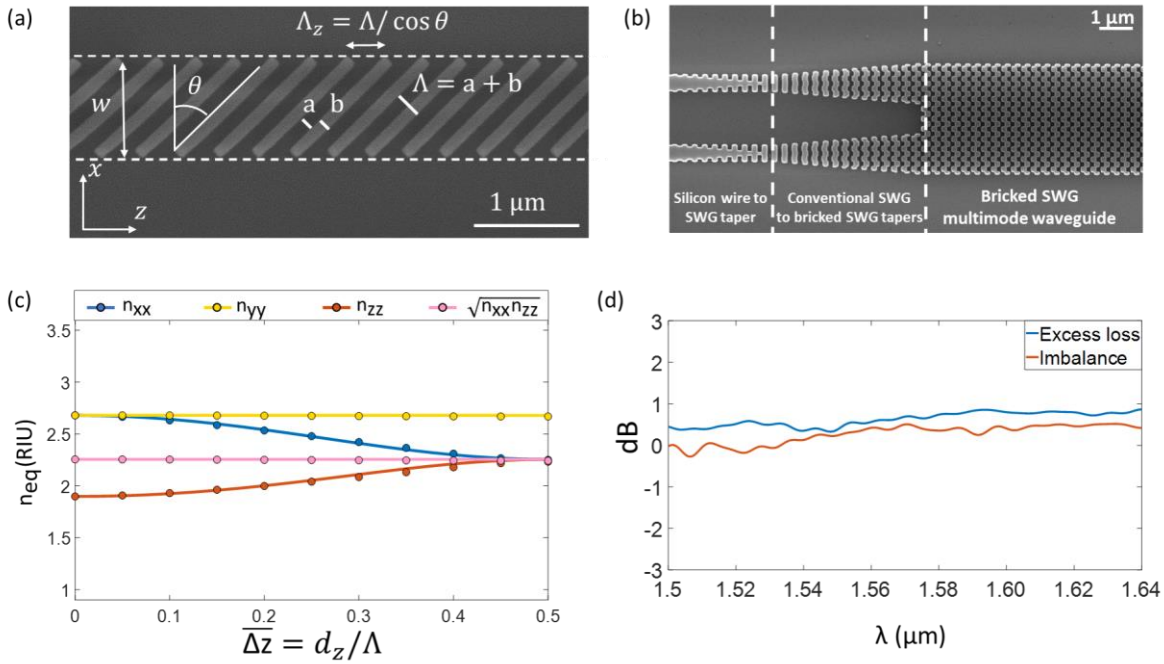

Figure 4. (a) SEM image of a tilted-SWG waveguide. (b) SEM image of a 2 × 2 bricked-SWG MMI. (c) Tensor components of a bricked-SWG waveguide as a function of the displacement d_z. (c) Excess loss and power imbalance of a 2 × 2 bricked-SWG MMI with a period length of 300 nm and a duty cycle of 50%.

6. SUSPENDED WAVEGUIDE FOR MID-INFRARED BAND

The mid-infrared band covers the wavelength range from 2 µm to 15 µm and offers interesting applications in sensing and free-space optical communications[40]. In addition, the feature sizes of nanophotonic structures scale up due to the increased operating wavelengths, which opens new venues for the development of SWG-engineered devices with easier fabrication. The popular silicon-on-insulator platform cannot be used at long wavelengths (λ > 4 µm) because of the high material absorption of silicon dioxide[40]. To overcome this problem, new waveguide platforms have been proposed, including silicon on sapphire[41], silicon on nitride[42], or germanium on silicon[43]. In order to push the operation limit up to λ ~ 8 µm, we proposed structurally suspending silicon-on-insulator waveguides by removing the lossy silicon dioxide[44]: first, a periodic series of holes are patterned at the subwavelength scale along the propagation direction, thus defining a waveguide core with a subwavelength lateral cladding; then, the sample is dipped in a hydrofluoric acid solution that removes the silicon dioxide underneath. The lateral SWG cladding gives access to the oxide layer, mechanically supports the waveguide core, and behaves as an equivalent homogeneous material that provides index contrast. Recently, to extend the operation window at even longer wavelengths, we have proposed the use of germanium, transparent up to λ ~ 15 µm, instead of silicon[45]. Figure 5(a) shows an SEM image of a suspended germanium waveguide operating at a wavelength of 7.7 µm. The waveguide was characterized using the cut-back method: suspended germanium micro-antennas were used to couple light in/out of the chip[46], and the power transmitted through a set of waveguides of different lengths was measured. As shown in Fig. 5(b), a propagation loss of ~5 dB/cm was obtained. Our simulations show that this platform can be easily optimized to work at longer wavelengths (potentially up to ~15 µm). Compared to silicon and germanium membranes than utilize ribs and hence require two dry etch steps[47,48], our proposed platform offers a simpler fabrication.

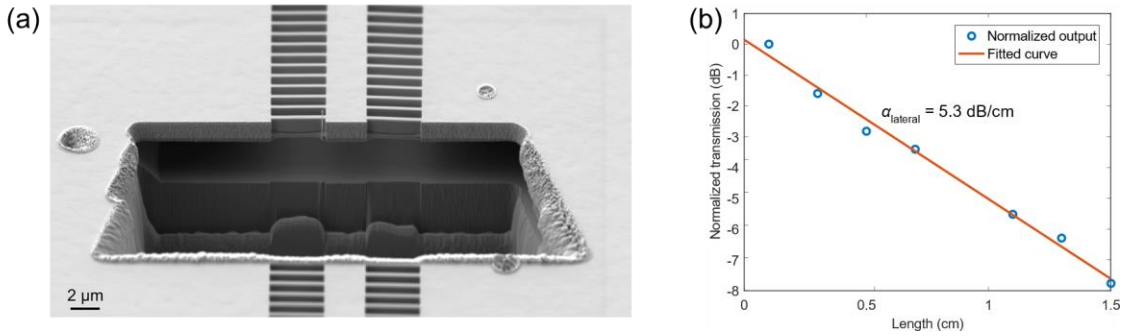

Figure 5. (a) SEM image of a suspended germanium waveguide. (b) Transmitted power as a function of the waveguide length, showing a propagation loss of ~5 dB/cm at a wavelength of 7.7 μm for TE polarization.

REFERENCES

[1] Cheben, P., Janz, S., Xu, D.-X., Lamontagne, B., Delage, A.., Tanev, S., "A broad-band waveguide grating coupler with a subwavelength grating mirror," IEEE Photonics Technol. Lett. **18**(1), 13–15 (2006).

[2] Cheben, P., Halir, R., Schmid, J. H., Atwater, H. A.., Smith, D. R., "Subwavelength integrated photonics," Nature **560**(7720), 565–572 (2018).

[3] Halir, R., Ortega-Moñux, A., Benedikovic, D., Mashanovich, G. Z., Wangüemert-Pérez, J. G., Schmid, J. H., Molina-Fernández, Í.., Cheben, P., "Subwavelength-grating metamaterial structures for silicon photonic devices," Proc. IEEE **106**(12), 2144–2157 (2018).

[4] Luque-González, J. M., Sánchez-Postigo, A., Hadij-ElHouati, A., Ortega-Moñux, A., Wangüemert-Pérez, J. G., Schmid, J. H., Cheben, P., Molina-Fernández, Í.., Halir, R., "A review of silicon subwavelength gratings: building break-through devices with anisotropic metamaterials," Nanophotonics **10**(11), 2765–2797 (2021).

[5] https://www.degruyter.com/document/doi/10.1515/nanoph-2021-0110/downloadAsset/suppl/j_nanoph-2021-0110_suppl.zip

[6] Sánchez-Postigo, A., Halir, R., Wangüemert-Pérez, J. G., Ortega-Moñux, A., Wang, S., Vachon, M., Schmid, J. H., Xu, D., Cheben, P., et al., "Breaking the Coupling Efficiency–Bandwidth Trade-Off in Surface Grating Couplers Using Zero-Order Radiation," Laser Photon. Rev., 2000542 (2021).

[7] Luque-González, J. M., Halir, R., Wangüemert-Pérez, J. G., De-Oliva-Rubio, J., Schmid, J. H., Cheben, P., Molina-Fernández, Í.., Ortega-Moñux, A., "An Ultracompact GRIN-Lens-Based Spot Size Converter using Subwavelength Grating Metamaterials," Laser Photon. Rev. **13**(11), 1900172 (2019).

[8] Gonzalo Wangüemert-Pérez, J., Cheben, P., Ortega-Moñux, A., Alonso-Ramos, C., Pérez-Galacho, D., Halir, R., Molina-Fernández, I., Xu, D.-X.., Schmid, J. H., "Evanescent field waveguide sensing with subwavelength grating structures in silicon-on-insulator," Opt. Lett. **39**(15), 4442–4445 (2014).

[9] Donzella, V., Sherwali, A., Flueckiger, J., Grist, S. M., Fard, S. T.., Chrostowski, L., "Design and fabrication of SOI micro-ring resonators based on sub-wavelength grating waveguides," Opt. Express **23**(4), 4791–4803 (2015).

[10] Torrijos-Morán, L., Griol, A.., García-Rupérez, J., "Experimental study of subwavelength grating bimodal waveguides as ultrasensitive interferometric sensors," Opt. Lett. **44**(19), 4702–4705 (2019).

[11] Wangüemert-Pérez, J. G., Hadij-ElHouati, A., Sánchez-Postigo, A., Leuermann, J., Xu, D.-X., Cheben, P., Ortega-Moñux, A., Halir, R.., Molina-Fernández, Í., "[INVITED] Subwavelength structures for silicon photonics biosensing," Opt. Laser Technol. **109**, 437–448 (2019).

[12] Xu, L., Wang, Y., Kumar, A., Patel, D., El-Fiky, E., Xing, Z., Li, R.., Plant, D. V., "Polarization Beam Splitter Based on MMI Coupler With SWG Birefringence Engineering on SOI," IEEE Photonics Technol. Lett. **30**(4), 403–406 (2018).

[13] Xu, H., Dai, D.., Shi, Y., "Ultra-Broadband and Ultra-Compact On-Chip Silicon Polarization Beam Splitter by Using Hetero-Anisotropic Metamaterials," Laser Photon. Rev. **13**(4), 1800349 (2019).

[14] Xu, H., Dai, D.., Shi, Y., "Anisotropic metamaterial-assisted all-silicon polarizer with 415-nm bandwidth," Photonics Res. **7**(12), 1432–1439 (2019).

[15] Poulton, C. V., Yaacobi, A., Cole, D. B., Byrd, M. J., Raval, M., Vermeulen, D.., Watts, M. R., "Coherent solid-state LIDAR with silicon photonic optical phased arrays," Opt. Lett. **42**(20), 4091–4094 (2017).
[16] Kim, T., Ngai, T., Timalsina, Y., Watts, M. R., Stojanovic, V., Bhargava, P., Poulton, C. V., Notaros, J., Yaacobi, A., et al., "A Single-Chip Optical Phased Array in a Wafer-Scale Silicon Photonics/CMOS 3D-Integration Platform," IEEE J. Solid-State Circuits **54**(11), 3061–3074 (2019).
[17] Miller, S. A., Chang, Y.-C., Phare, C. T., Shin, M. C., Zadka, M., Roberts, S. P., Stern, B., Ji, X., Mohanty, A., et al., "Large-scale optical phased array using a low-power multi-pass silicon photonic platform," Optica **7**(1), 3–6 (2020).
[18] Ma, W., Tan, S., Wang, K., Guo, W., Liu, Y., Liao, L., Zhou, L., Zhou, J., Li, X., et al., "Practical two-dimensional beam steering system using an integrated tunable laser and an optical phased array," Appl. Opt. **59**(32), 9985–9994 (2020).
[19] Tamir, T.., Peng, S. T., "Analysis and design of grating couplers," Appl. Phys. **14**(3), 235–254 (1977).
[20] Luan, E., Donzella, V., Cheung, K.., Chrostowski, L., "Advances in Silicon Photonic Sensors Using Sub-Wavelength Gratings," 2019 24th Optoelectron. Commun. Conf. 2019 Int. Conf. Photonics Switch. Comput., 1–3, IEEE (2019).
[21] Ginel-Moreno, P., Pereira-Martín, D., Hadij-ElHouati, A., Ye, W. N., Melati, D., Xu, D.-X., Janz, S., Ortega-Moñux, A., Wangüemert-Pérez, J. G., et al., "Highly efficient optical antenna with small beam divergence in silicon waveguides," Opt. Lett. **45**(20), 5668–5671 (2020).
[22] Ginel-Moreno, P., Sánchez-Postigo, A., De-Oliva-Rubio, J., Hadij-ElHouati, A., Ye, W. N., Wangüemert-Pérez, J. G., Molina-Fernández, Í., Schmid, J. H., Cheben, P., et al., "Millimeter-long metamaterial surface-emitting antenna in the silicon photonics platform," Opt. Lett. **46**(15), 3733–3736 (2021).
[23] Wang, X., Shi, W., Vafaei, R., Jaeger, N. A. F.., Chrostowski, L., "Uniform and Sampled Bragg Gratings in SOI Strip Waveguides with Sidewall Corrugations," IEEE Photonics Technol. Lett. (2011).
[24] Cheng, R.., Chrostowski, L., "Apodization of Silicon Integrated Bragg Gratings Through Periodic Phase Modulation," IEEE J. Sel. Top. Quantum Electron. **26**(2), 1–15 (2020).
[25] Pereira-Martín, D., Luque-González, J. M., Gonzalo Wangüemert-Pérez, J., Hadij-ElHouati, A., Molina-Fernández, Í., Cheben, P., Schmid, J. H., Wang, S., Ye, W. N., et al., "Complex spectral filters in silicon waveguides based on cladding-modulated Bragg gratings," Opt. Express **29**(11), 15867–15881 (2021).
[26] Skaar, J., Ligang Wang., Erdogan, T., "On the synthesis of fiber Bragg gratings by layer peeling," IEEE J. Quantum Electron. **37**(2), 165–173 (2001).
[27] Hao, Y., Wu, Y., Yang, J., Jiang, X.., Wang, M., "Novel dispersive and focusing device configuration based on curved waveguide grating (CWG)," Opt. Express **14**(19), 8630–8637 (2006).
[28] Bock, P. J., Cheben, P., Delâge, A., Schmid, J. H., Xu, D.-X., Janz, S.., Hall, T. J., "Demultiplexer with blazed waveguide sidewall grating and sub-wavelength grating structure," Opt. Express **16**(22), 17616–17625 (2008).
[29] Bock, P. J., Cheben, P., Schmid, J. H., Velasco, A. V., Delâge, A., Janz, S., Xu, D.-X., Lapointe, J., Hall, T. J., et al., "Demonstration of a curved sidewall grating demultiplexer on silicon," Opt. Express **20**(18), 19882–19892 (2012).
[30] Hadij-ElHouati, A., Cheben, P., Ortega-Moñux, A., Wangüemert-Pérez, J. G., Halir, R., Schmid, J. H.., Molina-Fernández, Í., "Distributed Bragg deflector coupler for on-chip shaping of optical beams," Opt. Express **27**(23), 33180–33193 (2019).
[31] Hadij-ElHouati, A., Cheben, P., Ortega-Moñux, A., Wangüemert-Pérez, J. G., Halir, R., De-Oliva-Rubio, J., Schmid, J. H.., Molina-Fernández, I., "High-efficiency conversion from waveguide mode to an on-chip beam using a metamaterial engineered Bragg deflector," Opt. Lett. **46**(10), 2409–2412 (2021).
[32] Hadij-ElHouati, A., Ortega-Moñux, A., Wangüemert-Pérez, J. G., Halir, R., Wang, S., Schmid, J. H., Cheben, P.., Molina-Fernández, I., "Low-loss off-axis curved waveguide grating demultiplexer," Opt. Lett. **46**(19), 4821–4824 (2021).
[33] Halir, R., Cheben, P., Luque-González, J. M., Sarmiento-Merenguel, J. D., Schmid, J. H., Wangüemert-Pérez, G., Xu, D.-X., Wang, S., Ortega-Moñux, A., et al., "Ultra-broadband nanophotonic beamsplitter using an anisotropic sub-wavelength metamaterial," Laser Photon. Rev. **10**(6), 1039–1046 (2016).
[34] Jahani, S., Kim, S., Atkinson, J., Wirth, J. C., Kalhor, F., Noman, A. Al., Newman, W. D., Shekhar, P., Han, K., et al., "Controlling evanescent waves using silicon photonic all-dielectric metamaterials for dense integration," Nat. Commun. **9**(1), 1893 (2018).
[35] González-Andrade, D., Luque-González, J. M., Gonzalo Wangüemert-Pérez, J., Ortega-Moñux, A., Cheben, P., Molina-Fernández, Í.., Velasco, A. V., "Ultra-broadband nanophotonic phase shifter based on subwavelength

metamaterial waveguides," Photonics Res. **8**(3), 359–367 (2020).
[36] Luque-González, J. M., Herrero-Bermello, A., Ortega-Moñux, A., Molina-Fernández, Í., Velasco, A. V., Cheben, P., Schmid, J. H., Wang, S.., Halir, R., "Tilted subwavelength gratings: controlling anisotropy in metamaterial nanophotonic waveguides," Opt. Lett. **43**(19), 4691–4694 (2018).
[37] Herrero-Bermello, A., Dias-Ponte, A., Luque-González, J. M., Ortega-Moñux, A., Velasco, A. V., Cheben, P.., Halir, R., "Experimental demonstration of metamaterial anisotropy engineering for broadband on-chip polarization beam splitting," Opt. Express **28**(11), 16385–16393 (2020).
[38] Luque-González, J. M., Herrero-Bermello, A., Ortega-Moñux, A., Sánchez-Rodríguez, M., Velasco, A. V., Schmid, J. H., Cheben, P., Molina-Fernández, Í.., Halir, R., "Polarization splitting directional coupler using tilted subwavelength gratings," Opt. Lett. **45**(13), 3398–3401 (2020).
[39] Luque-González, J. M., Ortega-Moñux, A., Halir, R., Schmid, J. H., Cheben, P., Molina-Fernández, Í.., Wangüemert-Pérez, J. G., "Bricked Subwavelength Gratings: A Tailorable On-Chip Metamaterial Topology," Laser Photon. Rev. **15**(6), 2000478 (2021).
[40] Soref, R., "Mid-infrared photonics in silicon and germanium," Nat. Photonics **4**, 495–497, Nature Publishing Group (2010).
[41] Baehr-Jones, T., Spott, A., Ilic, R., Spott, A., Penkov, B., Asher, W.., Hochberg, M., "Silicon-on-sapphire integrated waveguides for the mid-infrared," Opt. Express **18**(12), 12127–12135 (2010).
[42] Khan, S., Chiles, J., Ma, J.., Fathpour, S., "Silicon-on-nitride waveguides for mid- and near-infrared integrated photonics," Appl. Phys. Lett. **102**(12), 121104 (2013).
[43] Gallacher, K., Millar, R. W., Griškevičiūte, U., Baldassarre, L., Sorel, M., Ortolani, M.., Paul, D. J., "Low loss Ge-on-Si waveguides operating in the 8–14 um atmospheric transmission window," Opt. Express **26**(20), 25667–25675 (2018).
[44] Sánchez-Postigo, A., Wangüemert-Pérez, J. G., Soler Penadés, J., Ortega-Moñux, A., Nedeljkovic, M., Halir, R., El Mokhtari Mimun, F., Xu Cheng, Y., Qu, Z., et al., "Mid-infrared suspended waveguide platform and building blocks," IET Optoelectron. **13**(2), 55–61 (2019).
[45] Sánchez-Postigo, A., Ortega-Moñux, A., Soler Penades, J., Osman, A., Nedeljkovic, M., Qu, Z., Wu, Y., Molina-Fernández, I., Cheben, P., et al., "Suspended germanium waveguides with subwavelength-grating metamaterial cladding for the mid-infrared band," Opt. Express **29**(11), 16867–16878 (2021).
[46] Sánchez-Postigo, A., Ortega-Moñux, A., Pereira-Martín, D., Molina-Fernández, Í., Halir, R., Cheben, P., Soler Penadés, J., Nedeljkovic, M., Mashanovich, G. Z., et al., "Design of a suspended germanium micro-antenna for efficient fiber-chip coupling in the long-wavelength mid-infrared range," Opt. Express **27**(16), 22302–22315 (2019).
[47] Cheng, Z., Zhou, W., Xiao, T.-H., Tsang, H. K., Takenaka, M., Set, S. Y., Zhao, Z., Chang, C.-Y.., Goda, K., "Mid-infrared high-Q germanium microring resonator," Opt. Lett. **43**(12), 2885 (2018).
[48] Osman, A., Nedeljkovic, M., Soler Penades, J., Wu, Y., Qu, Z., Khokhar, A. Z., Debnath, K.., Mashanovich, G. Z., "Suspended low-loss germanium waveguides for the longwave infrared," Opt. Lett. **43**(24), 5997–6000 (2018).